Application of the Regularized Shallow Water Equations for Numerical Simulation of Seiche Level Oscillations in the Sea of Azov

T. G. Elizarova[a], * **and D. S. Saburin**[b], **

[a]Keldysh Institute of Applied Mathematics, Russian Academy of Sciences, Moscow, Russia
[b]Faculty of Physics, Moscow State University, Moscow, Russia
*e-mail: telizar@mail.ru,
**e-mail: saburin@physics.msu.ru
Received March 28, 2016

Abstract—A mathematical model for calculating the currents in the sea area scale was developed for the first time within an algorithm of regularized shallow water equations. The model and the numerical algorithm are described as applied to the topology and natural features of the Sea of Azov. The results of the calculations of hydrodynamic currents in the Sea of Azov in the presence of typical seiche waves caused by tidal or wind influences are presented.

INTRODUCTION

The Azov region is a strategically important region for the Russian Federation: it has enormous transport, industrial, recreational, strategic, and military significance. Therefore, forecasting the dynamics and circulation of the sea at varied environmental impacts, primarily due to weather variations, is considered to be a priority problem. The Sea of Azov is distinguished for its unique topography and climate. Some climatic phenomena, mostly caused by strong winds, can bring about serious risks for people and develop to the scale of disasters. They include tidal and wind-generated oscillations of the sea level, storm winds caused by cyclonic activity, storm waves, seiches, tsunamis, and wind waves. Each of these phenomena imposes its requirements on the numerical simulations elaborated to study and forecast them.

Seiches are standing waves emerging in an enclosed or partially enclosed body of water under the action of atmospheric pressure variations, winds, or storm surges from neighboring basins.

In the shallow Sea of Azov, seiche waves are frequent. Currents emerging due to seiches set the total water mass of the basin in motion. At the nodal points with an almost constant water level and in narrow spots, seiches can induce extreme current velocities of up to 1.5 m/s. The amplitude of level oscillations can exceed 1 m. Seiches can significantly enhance wind-generated effects in this region, and induce catastrophic water level differentials. The detailed description of these phenomena in the Sea of Azov is presented, for example, in [1]. Therefore, studying and forecasting seiche currents in the shallow Sea of Azov with its gently sloping shores are quite relevant.

At present, there are some highly precise simulations describing the Azov hydrodynamics presented in [2–9] and references in them. These numerical simulations use various two-dimensional, three-dimensional, single-layer, and two-layer finite-difference algorithms, which are solved by various numerical methods, including the explicit and implicit finite-difference approximations, and the application of spaced and nonuniform grids and finite element methods.

The approach offered by the authors is based on two-dimensional shallow water equations. A new numerical method for shallow water equations was offered and tested in [10] based on classical equation smoothing over a small time interval. This procedure leads to the creation of regularizing additives, which ensure the stability of the numerical solution of the problem for a wide range of parameters. This approach is expanded to nonstructured grids and can be naturally processed in parallel over the computational cluster. An important advantage of the algorithm is its generalization for the cases of flows that promote the
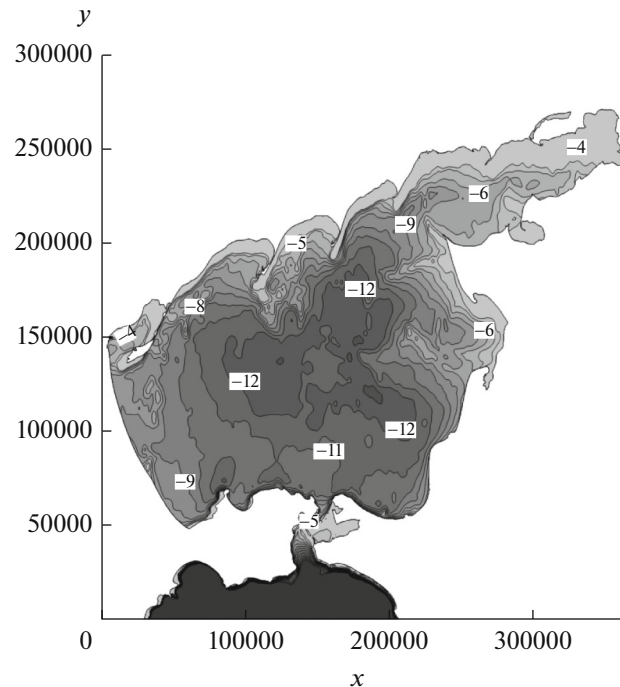
Fig. 1. Azov seabed topography (depth indicated in m).

emergence and disappearance of dry dry bottom areas; i.e., they generate the so-called drying and flooding zones [11]. The approach was used, in particular, for the numerical simulation of liquid fluctuations in freighter reservoirs [12, 13] and simulation of the experimentally observed formation of a soliton on a water surface under the impact of wind in the annular tunnel [14].

In this paper, the regularized shallow water equations are used for the first time for the numerical simulation of currents in the sea area scale. Calculations of the standard for the Sea of Azov seiche waves are presented as an example. Under natural conditions, these oscillations most frequently emerge due to the persistent pressure of a constantly directed wind, which shapes the initial gradient of the sea surface level.

1. STATEMENT OF THE PROBLEM IN THE SHALLOW WATER EQUATIONS

One of the features of the sea and ocean hydrodynamic problems is that the aquatic environment layer is quite thin and its depth is much smaller than its longitudinal dimensions. This is widely used for building baroclinic circulation models in the seas and the entire world ocean (see, for example, papers [15, 16] and the bibliography to them). However, a simpler hydrodynamic approach of shallow water is suitable for describing some problems [17]. Within this approach, the vertical component of the flows velocity in the layer is neglected, and the longitudinal velocities are assumed constant over its depth.

We consider a two-dimensional set of shallow water equations in flux form. We take into consideration the force of the wind, the Coriolis force, and the seabed friction force as external forces. Having in mind these forces and the topology of the seabed, we can write the following system:

$$\frac{\partial h}{\partial t} + \frac{\partial u_x h}{\partial x} + \frac{\partial u_y h}{\partial y} = 0,$$

$$\frac{\partial u_x h}{\partial t} + \frac{\partial}{\partial x}\left(hu_x^2 + \frac{1}{2}gh^2\right) + \frac{\partial}{\partial y}(hu_x u_y) = hf^c u_y - gh\frac{\partial b}{\partial x} + \tau^{x,w} - \tau^{x,b}, \tag{1}$$

$$\frac{\partial u_y h}{\partial t} + \frac{\partial}{\partial x}(hu_x u_y) + \frac{\partial}{\partial y}\left(hu_y^2 + \frac{1}{2}gh^2\right) = -hf^c u_x - gh\frac{\partial b}{\partial y} + \tau^{y,w} - \tau^{y,b}.$$
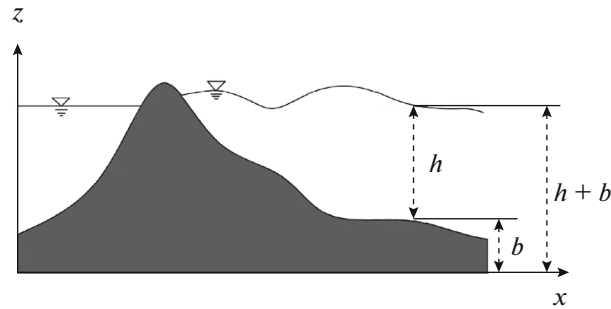
Fig. 2. Outline of variable shallow water equations.

Here $h(x, y, t)$ is the liquid height above the seabed level, $u_x(x, y, t)$ and $u_y(x, y, t)$ are the components of the flow velocity, g is the gravitational acceleration and function $b(x, y)$ describes the seabed topography (Figs. 1, 2).

Projections of the force of wind friction against the water surface are designated as τ^w and calculated as $\tau^{i,w} = \gamma|W|W_i$, where W_i is the wind component, $|W| = \sqrt{W_x^2 + W_y^2}$ is the wind velocity module, and γ is the coefficient of wind friction against the free water surface.

Projections of the force of water friction against the seabed are designated as τ^b and calculated by relation $\tau^{i,b} = \mu|u|u_i$, where μ is the friction coefficient and $|u| = \sqrt{u_x^2 + u_y^2}$ is the flow velocity module.

Friction coefficients are preset values, and for sea areas they are $\mu = 2.6 \times 10^{-3}$ [8] and $\gamma = 3.25 \times 10^{-6}$ [16]. Wind velocity is also set based on the in-field observations and can be time dependent.

The right parts of the equations of motion include the Coriolis force f^{cor} with components $f_x^{cor} = f^c u_y$ and $f_y^{cor} = -f^c u_x$, where $f_c = 2\Omega \sin\phi = 2\dfrac{2\pi}{T}\sin\phi$ is the Coriolis parameter, $\Omega = 2\pi/T = 7.2921 \times 10^{-5}\,\text{s}^{-1}$ is the angular speed of the Earth's rotation, $T = 86400$ is the diurnal period of the Earth's rotation measured in s, and ϕ is the point latitude in degrees counted from the equator.

The scope of the problem represented in Fig. 1 covers the Sea of Azov area, the Kerch Strait, and the adjacent part of the Black Sea. The inclusion of the Kerch Strait in the scope allows us to evaluate the impact of the seiche waves of the Sea of Azov on the surface levels and currents in the zone of the strait.

The studied region is located within the limits from $34°45'6''$ E to $39°29'38''$ E, and from $44°48'4''$ N to $47°16'12''$ N, respectively. The seabed topology is studied set on the grid with a resolution of $8''$. Due to the rather small linear dimensions of the Sea of Azov in relation to the Earth's radius, the problem is set in Cartesian coordinates. A uniform rectangular grid with a resolution of 250×250 m is used. The coastline corresponding to the undisturbed sea level is chosen as the zero mark.

The observations show that in the Sea of Azov, the impact of a long-term (for several days) unidirectional wind can generate a surface level gradient, whose destruction produces a seiche. This seiche is an analog of a standing wave inside a pool. Below an example is given of the calculations of the surface level's evolution and the current velocity for the standard seiche wave with the initial amplitude of one meter.

2. REGULARIZED SHALLOW WATER EQUATIONS

The regularization method mentioned above in the Introduction applied to Navier–Stokes and Euler equations provides an opportunity to write effective numerical algorithms for their solution, which are stated, for example, in [18–20].

The regularized shallow water equations and the technique of their formulation are described in [10]. Below we present the obtained equations taking friction forces and Coriolis force into account. Regularized equations (1) appear as

$$\frac{\partial h}{\partial t} + \frac{\partial j_{mx}}{\partial x} + \frac{\partial j_{my}}{\partial y} = 0,$$

$$\frac{\partial h u_x}{\partial t} + \frac{\partial j_{mx} u_x}{\partial x} + \frac{\partial j_{my} u_x}{\partial y} + \frac{\partial}{\partial x}\left(\frac{gh^2}{2}\right) = h^*\left(f^c u_y - g\frac{\partial b}{\partial x}\right) + \frac{\partial \Pi_{xx}}{\partial x} + \frac{\partial \Pi_{yx}}{\partial y} + \tau^{x,w} - \tau^{x,b},$$

$$\frac{\partial h u_y}{\partial t} + \frac{\partial j_{mx} u_y}{\partial x} + \frac{\partial j_{my} u_y}{\partial y} + \frac{\partial}{\partial y}\left(\frac{gh^2}{2}\right) = h^*\left(-f^c u_x - g\frac{\partial b}{\partial y}\right) + \frac{\partial \Pi_{xy}}{\partial x} + \frac{\partial \Pi_{yy}}{\partial y} + \tau^{y,w} - \tau^{y,b}. \tag{2}$$

Parameters j_{mx} and j_{my} have the physical sense of a regularized liquid flux and are expressed as

$$j_{mx} = h(u_x - w_x), \quad j_{my} = h(u_y - w_y), \tag{3}$$

where hu_i is the liquid flow within the shallow water approximation, and w_i is the regularizing correction of velocity expressed as

$$w_x = \frac{\tau}{h}\left(\frac{\partial(h u_x^2)}{\partial x} + \frac{\partial(h u_x u_y)}{\partial y} + gh\frac{\partial(h+b)}{\partial x}\right),$$

$$w_y = \frac{\tau}{h}\left(\frac{\partial(h u_x u_y)}{\partial x} + \frac{\partial(h u_y^2)}{\partial y} + gh\frac{\partial(h+b)}{\partial y}\right). \tag{4}$$

The components of tensor $\Pi_{i,j}$ appear as follows:

$$\Pi_{xx} = u_x w_x^* + R^* + \Pi_{NSxx}, \quad \Pi_{yx} = u_y w_x^* + \Pi_{NSyx},$$

$$\Pi_{xy} = u_x w_y^* + \Pi_{NSxy}, \quad \Pi_{yy} = u_y w_y^* + R^* + \Pi_{NSyy}, \tag{5}$$

where

$$w_x^* = \tau h\left(u_x \frac{\partial u_x}{\partial x} + u_y \frac{\partial u_x}{\partial y} + g\frac{\partial(h+b)}{\partial x}\right), \quad w_y^* = \tau h\left(u_x \frac{\partial u_y}{\partial x} + u_y \frac{\partial u_y}{\partial y} + g\frac{\partial(h+b)}{\partial y}\right),$$

$$R^* = g\tau h\left(\frac{\partial h u_x}{\partial x} + \frac{\partial h u_y}{\partial y}\right).$$

Compared with the classical equations in the shallow water approximation, new small terms emerge here, whose magnitude is about $O(\tau)$. To smooth the numerical solution, Navier–Stokes viscous stress tensor components are also used, in which the coefficient of viscosity is connected with parameter τ. These components are added to $\Pi_{i,j}$ (5) and appear as

$$\Pi_{NSxx} = \tau\frac{gh^2}{2}2\frac{\partial u_x}{\partial x}, \quad \Pi_{NSxy} = \tau\frac{gh^2}{2}\left(\frac{\partial u_x}{\partial y} + \frac{\partial u_y}{\partial x}\right), \quad \Pi_{NSyy} = \tau\frac{gh^2}{2}2\frac{\partial u_y}{\partial y}.$$

Parameter h^* appears as

$$h^* = h - \tau\left(\frac{\partial h u_x}{\partial x} + \frac{\partial h u_y}{\partial y}\right). \tag{6}$$

The system of equations (2)–(6) is closely connected with the initial system of shallow water equations and at $\tau = 0$ transforms into system (1). The appearance of components containing the coefficient τ is determined by the appearance of the initial equations; therefore the stationary solutions of the initial system (1) are the stationary solutions of system (2)–(6). One of these solutions is the solution of the "steady lake" problem. Studies of numerous connections between regularized equations and their classical analogs are presented, in particular, in [21, 22].

The reflection conditions for h have been taken as the boundary conditions for shallow water regularized equations, taking into consideration the seabed topology and the condition of the absence of a flow in the remaining part of the zone, in the following form:

$$\frac{\partial(h+b)}{\partial n} = 0, \quad \frac{\partial u_\tau}{\partial n} = 0, \quad u_n = 0, \quad \frac{\partial u_\tau}{\partial n} = 0, \quad \frac{\partial u_n}{\partial n} = 0.$$

Depending on the boundary location, index n designates the derivative with respect to x or y normal to the boundary, and index τ designates the tangential component of the velocity vector at the region's boundary, i.e., u_x or u_y.

3. DIFFERENCE ALGORITHM

The explicit in time finite-difference algorithm, which uses the integrointerpolation method with the spatial derivative approximation in the flux form by central differences, is used for the numerical solution of the system of equations (2)−(6). Uniform spatial grids are used in the calculations.

The values of $h(x, y, t)$ and $u(x, y, t)$ are set in the nodes of the spatial grid (i, j), the values at half-integer points $i \pm 1/2, j$ and $i, j \pm 1/2$ are calculated as the arithmetical means of the values in the adjacent nodes, for example, $h_{i\pm1/2,j} = 0.5(h_{i,j} + h_{i\pm1,j})$. The values in the centers of the cells are determined as the arithmetical means of the values in the adjacent nodes, for example, $h_{i+1/2,j+1/2} = 0.25(h_{i,j} + h_{i+1,j} + h_{i,j+1} + h_{i+1,j+1})$. The values u_x, u_y, and b are approximated in the same way. Flux values on the template edges are determined via regularizing additives:

$$j^x_{i\pm1/2,j} = h_{i\pm1/2,j}(u^x_{i\pm1/2,j} - w^x_{i\pm1/2,j}), \quad j^y_{i,j\pm1/2} = h_{i,j\pm1/2}(u^y_{i,j\pm1/2} - w^y_{i,j\pm1/2}). \tag{7}$$

Hereinafter, for convenience, the upper index is used to designate the x and y components. The values $w^x_{i+1/2,j}$, $w^x_{i-1/2,j}$ and $w^y_{i,j+1/2}$, $w^y_{i,j+1/2}$ are also determined on the template edges. The derivatives included in these expressions are approximated by the central differences. The difference designation of these values is displayed in [11].

Values $\Pi_{i,j}$ are determined using regularizing additives, similar to (7). Let us exemplify the difference approximation of $w^{*,x}$:

$$w^{*,x}_{i+1/2,j} = \tau_{i+1/2,j} h_{i+1/2,j} \left(u^x_{i+1/2,j} \frac{u^x_{i+1,j} - u^x_{i,j}}{\Delta x} \right.$$

$$\left. + u^y_{i+1/2,j} \frac{u^x_{i+1/2,j+1/2} - u^x_{i+1/2,j-1/2}}{\Delta y} + g h_{i+1/2,j} \frac{h_{i+1,j} + b_{i+1,j} - h_{i,j} - b_{i,j}}{\Delta x} \right),$$

$$w^{*,x}_{i-1/2,j} = \tau_{i-1/2,j} h_{i-1/2,j} \left(u^x_{i-1/2,j} \frac{u^x_{i,j} - u^x_{i-1,j}}{\Delta x} \right.$$

$$\left. + u^y_{i-1/2,j} \frac{u^x_{i-1/2,j+1/2} - u^x_{i-1/2,j-1/2}}{\Delta y} + g h_{i-1/2,j} \frac{h_{i,j} + b_{i,j} - h_{i-1,j} - b_{i-1,j}}{\Delta x} \right),$$

$$w^{*,x}_{i,j+1/2} = \tau_{i,j+1/2} h_{i,j+1/2} \left(u^x_{i,j+1/2} \frac{u^x_{i+1/2,j+1/2} - u^x_{i-1/2,j+1/2}}{\Delta x} \right.$$

$$\left. + u^y_{i,j+1/2} \frac{u^x_{i,j+1} - u^x_{i,j}}{\Delta y} + g h_{i,j+1/2} \frac{h_{i+1/2,j+1/2} + b_{i+1/2,j+1/2} - h_{i-1/2,j+1/2} - b_{i-1/2,j+1/2}}{\Delta x} \right),$$

$$w^{*,x}_{i,j-1/2} = \tau_{i,j-1/2} h_{i,j-1/2} \left(u^x_{i,j-1/2} \frac{u^x_{i+1/2,j-1/2} - u^x_{i-1/2,j-1/2}}{\Delta x} \right.$$

$$\left. + u^y_{i,j-1/2} \frac{u^x_{i,j} - u^x_{i,j-1}}{\Delta y} + g h_{i,j-1/2} \frac{h_{i+1/2,j-1/2} + b_{i+1/2,j-1/2} - h_{i-1/2,j-1/2} - b_{i-1/2,j-1/2}}{\Delta x} \right).$$

A similar method is applied to approximate values $w^{*,y}$, R^*, and $\Pi_{i,j}^{NS}$. The difference approximation of h^* (6) ensuring the fulfillment of the well-balanced condition is presented in [11].

Applying the integrointerpolation method, we obtain the following time explicit finite-difference algorithm for the system of equations (2)−(6)

$$\hat{h}_{i,j} = h_{i,j} - \frac{\Delta t}{\Delta x}\left(j_{i+1/2,j}^x - j_{i-1/2,j}^x\right) - \frac{\Delta t}{\Delta y}\left(j_{i,j+1/2}^y - j_{i,j-1/2}^y\right),$$

$$\hat{h}_{i,j}\hat{u}_{i,j}^x = h_{i,j}u_{i,j}^x + \Delta t\left(\tau_{i,j}^{x,w} - \tau_{i,j}^{x,b}\right) + \frac{\Delta t}{\Delta x}\left(\Pi_{i+1/2,j}^{xx} - \Pi_{i-1/2,j}^{xx}\right)$$

$$- \frac{\Delta t}{\Delta x}\left(u_{i+1/2,j}^x j_{i+1/2,j}^x - u_{i-1/2,j}^x j_{i-1/2,j}^x\right) - 0.5g\frac{\Delta t}{\Delta x}(h_{i+1/2,j}^2 - h_{i-1/2,j}^2) + \frac{\Delta t}{\Delta y}\left(\Pi_{i,j+1/2}^{yx} - \Pi_{i,j-1/2}^{yx}\right)$$

$$- \frac{\Delta t}{\Delta y}\left(u_{i,j+1/2}^x j_{i,j+1/2}^y - u_{i,j-1/2}^x j_{i,j-1/2}^y\right) + \Delta t h_{x,i,j}^*\left(f^c u_{i,j}^y - g\frac{b_{i+1/2,j} - b_{i-1/2,j}}{\Delta x}\right),$$

$$\hat{h}_{i,j}\hat{u}_{i,j}^y = h_{i,j}u_{i,j}^y + \Delta t\left(\tau^{y,w} - \tau^{y,b}\right) + \frac{\Delta t}{\Delta x}\left(\Pi_{i+1/2,j}^{xy} - \Pi_{i-1/2,j}^{xy}\right)$$

$$- \frac{\Delta t}{\Delta x}\left(u_{i+1/2,j}^y j_{i+1/2,j}^x - u_{i-1/2,j}^y j_{i-1/2,j}^x\right) - 0.5g\frac{\Delta t}{\Delta y}(h_{i,j+1/2}^2 - h_{i,j-1/2}^2) + \frac{\Delta t}{\Delta y}\left(\Pi_{i,j+1/2}^{yy} - \Pi_{i,j-1/2}^{yy}\right)$$

$$- \frac{\Delta t}{\Delta y}\left(u_{i,j+1/2}^y j_{i,j+1/2}^y - u_{i,j-1/2}^y j_{i,j-1/2}^y\right) + \Delta t h_{y,i,j}^*\left(-f^c u_{i,j}^x - g\frac{b_{i,j+1/2} - b_{i,j-1/2}}{\Delta y}\right).$$

Here the values with diacriticals $\hat{h}$ and $\hat{u}$ relate to the upper temporary layer, Δt designates the time interval, and Δx and Δy are the intervals of a difference grid in space.

The numerical algorithm's stability is provided by the terms containing the coefficient τ, whose value is connected with the spatial grid resolution and can be calculated by the following expressions:

$$\tau = \alpha\frac{\Delta x + \Delta y}{2c}, \quad c = \sqrt{gh(x,y,t)},$$

where c is the velocity of propagation of the small disturbances calculated in the approximation of the shallow water model, $0 < \alpha < 1$ is the numerical coefficient chosen based on the conditions of the calculation's precision and stability. In the majority of calculations, $\alpha = 0.1$. The time interval is chosen in accordance with the Courant condition, which takes the following form for this problem:

$$\Delta t = \beta\frac{\Delta x + \Delta y}{2c_{\max}}.$$

The courant number $0 < \beta < 1$ depends on regularization parameter τ in the form of $\beta = \beta(\alpha)$ and is chosen in the process of the calculations to ensure the monotonicity of the numerical solution. In these calculations, $\beta = 0.5$.

Thus, the difference algorithm includes two configured parameters: Courant number β and regularization parameter α, which determine the precision and stability of the numerical solution.

4. REMARKS ABOUT THE NUMERICAL IMPLEMENTATION

The problem is considered in Cartesian coordinates on a uniform rectangular grid based on the existing topographical data of the Sea of Azov seabed and the adjacent territories. The grid step is $\Delta x = \Delta y = 250$ m. The grid contains $1521 \times 1091 = 1659411$ nodes. The time interval is $\Delta t = 10.4$ s.

The numerical approximation of the Coriolis force containing multiplier $\sin\phi$ depending on the latitude taken in the geocentric coordinate system is made without transformation of this multiplier into the Cartesian coordinate system. Within the difference algorithm, the values are calculated in every node of the grid with a constant interval of 8 seconds of latitude.

To simplify the calculations of the flow near the coastline, the coastline border was additionally raised by 5 m. This provided an opportunity to avoid calculating the dry seabed zone algorithm within the problem solution, since the presence of these zones has no significant influence on the seiche waves.
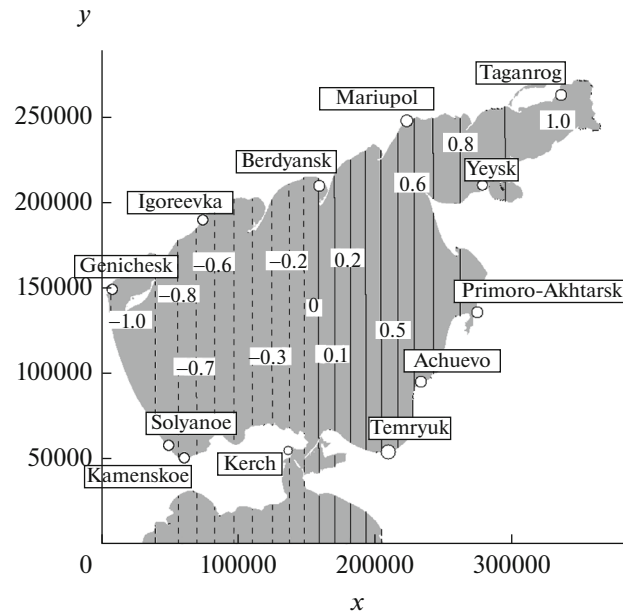
Fig. 3. Single-mode seiche in the Azov Basin, $t = 0$. Major ports of the Sea of Azov. Lines indicate the levels of deviation of the Sea of Azov's depth from the equilibrium; solid lines show the elevation levels, dashed lines show the depression levels.

The majority of the existing models describing the circulation of the seas and oceans use parameter η as an unknown thickness of the liquid layer counted from the equilibrium level of the stationary liquid level h_0, while axis Z is directed downwards. Thus, the sea surface level is assumed to be zero, and the sea depth is strictly positive. In the numerical algorithm used by the authors, the value taken as an unknown variable is the level height h counted from the seabed level with the topographical profile b. The maximum depth of the basin is taken as the zero mark; see Fig. 2. To visualize the data of the water surface level obtained from the calculations, the following formula is used:

$$\eta = h + b - \xi_0 = h - h_0,$$

where $\xi_0 = h_0 + b$ is the position of the liquid in a stationary well-balanced basin.

To test the equilibrium of the well-balanced finite-difference algorithm, the so-called steady lake problem was calculated. This problem stipulated a numerical proof of the obvious fact that in the absence of external influences (in this case, wind) the initially stationary surface of the basin $h_0 + b = \xi_0$ remained stationary, and the seabed's peculiarities did not cause nonphysical fluctuations. The calculations were carried out for two days. The maximum deviations from the equilibrium level were observed at the initial moment and reached about 1 cm. These fluctuations faded completely with time. The errors were small against the calculated fluctuations.

The initial conditions of the seiche problem are stated as follows. Let us assume that at the initial moment ($t = 0$), a uniform sea level gradient is set over the sea area, and it is +1 meter counting from the equilibrium value h_0 in the upper right part of the area and −1 meter in the lower left part. The numerical algorithm of setting this gradient is by dividing the interval from +1 meter to −1 meter into 1000 sublevels of equal area. This provides an opportunity to contain the total area of the liquid within the calculated zone. Fig. 3 shows the initial structure of the height in meters. We assume the liquid to be stationary at the initial time moment $u_x = u_y = 0$. In the calculations presented below, the wind velocity is also assumed to be zero.

The majority of the calculations were made during the time period of up to one week of real time.

The numerical calculation of a 72-hour time period takes about 8 hours of computer time on a PC with an Intel(R) Core(TM) i5 processor with a frequency 2.8 GHz. The program is written in the C language. The program has not been optimized, though optimization is potentially able to accelerate the calculation 3−5 times.
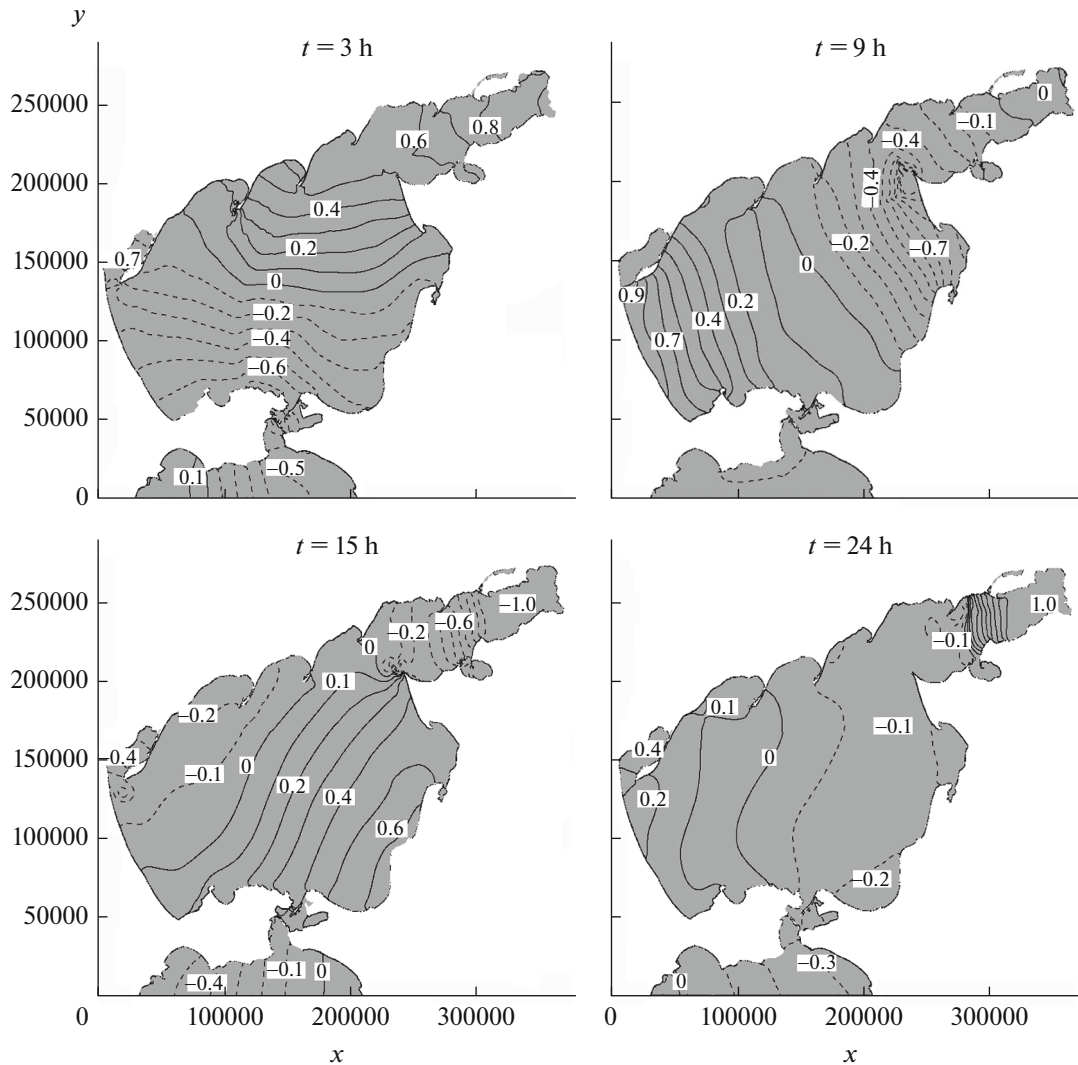
Fig. 4. Deviation η of surface level from the equilibrium in the Sea of Azov Basin.

5. THE RESULTS OF THE CALCULATIONS OF SEICHE WAVES

The first series of calculations of seiche waves was carried out without taking seabed friction into consideration ($\mu = 0$). The water level distribution as of four characteristic time moments $t = 3, 9, 15,$ and 24 hours from the start of the oscillations are displayed in Fig. 4. Figure 5 shows the respective streamlines.

The charts in Fig. 4 show the displacements of the maximum and minimum sea levels: thus, at $t = 0$, the maximum level is observed in the northeastern part of the Azov Sea, and the minimum level is in its western and southwestern parts; at $t = 3$ h, the maximum level is in the northern and northwestern part of the sea, while the minimum level is in the southeastern part of the region; at $t = 9$ h, the maximum level is in the southern part of the region, while the minimum level is in its northern and northeastern parts; at $t = 15$ h, the maximum level is in the eastern part of the region, and the minimum level is in the western and northeastern (in Taganrog bay) parts; and finally, at $t = 24$ h, the maximum level is again in the northeastern and western parts of the sea, and the minimum level is in the eastern and central parts. Thus, in 18−24 hours, the maximum became the minimum and vice versa in each zone, which indicates the presence of water mass being periodically displaced counterclockwise in the sea area. This circular displacement is stipulated by the Coriolis effect.

Figure 5 shows a complex nonstationary circulation throughout the water area. The main streamline directions also move counterclockwise: at $t = 3$ h, they are directed from the east to the west; at $t = 9$ h, the direction changes from the north to the south; at $t = 15$ h, they are directed from the south to the
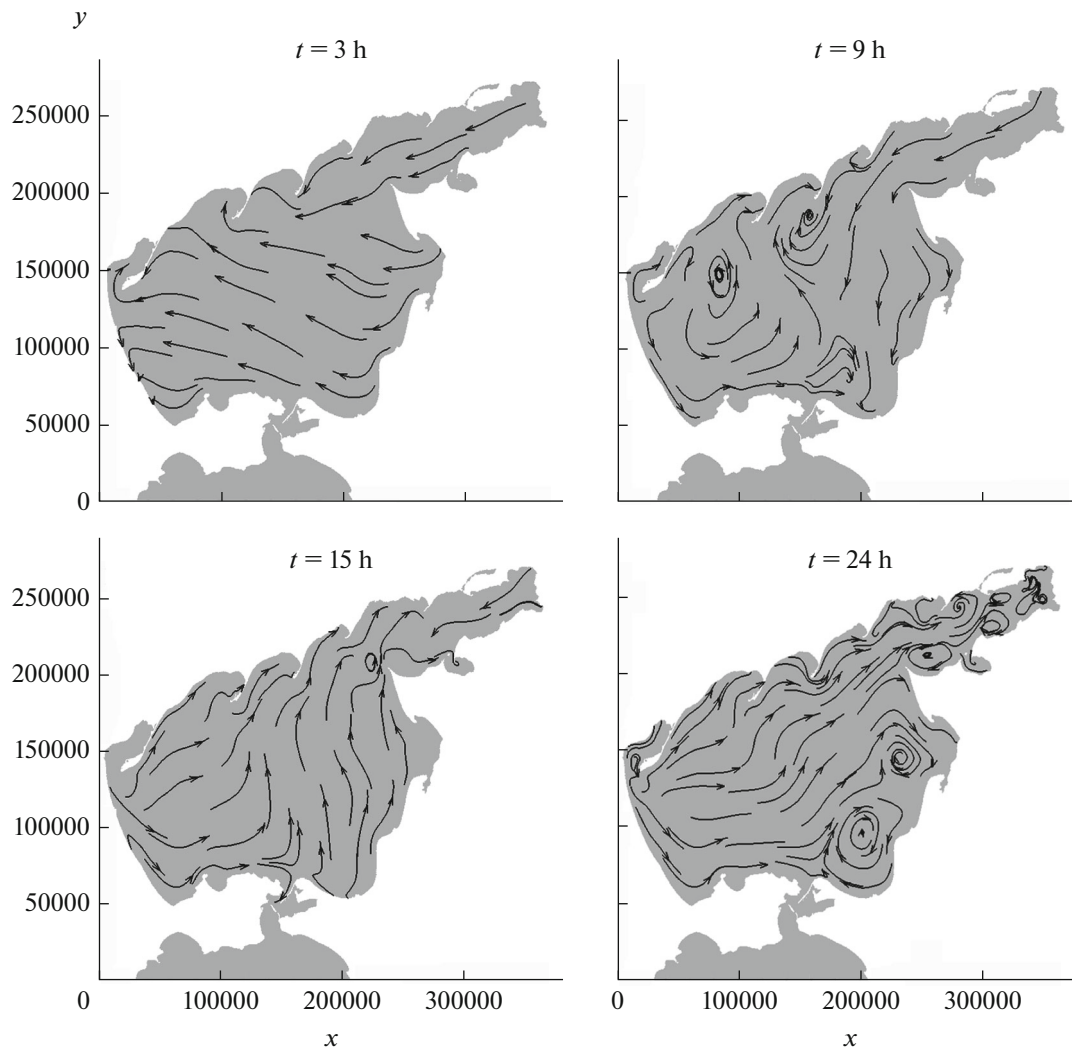
Fig. 5. Streamlines in the presence of seiche waves in the Sea of Azov.

north; and at $t = 24$ h, they are directed from the west to the east. The strongest currents are observed in Taganrog Bay.

Figures 4 and 5 show that, in different regions of the sea area, the periods of level oscillations are different and depend on the location. Studies of the displacement of the surface levels and currents in the main ports of the Sea of Azov (their locations are shown in Fig. 3) are of practical interest. We show the main features of the evolution of the sea level for four cities located in different parts of the Sea of Azov: Genichesk, Taganrog, Kerch, and Berdyansk. The respective curves are designated by the solid lines.

Below, graphs of the sea level's evolution are presented for every hour over 72 hours. We start our studies in Taganrog, located in the northeastern part of the region. We fix a point with coordinates $x = 337432$ m and $y = 262004$ m, which corresponds to the location of Taganrog port. The level oscillations observed at the point with time are shown in Fig. 6. Here and in following graphs, axis x corresponds to the time (in hours) of the profile's evolution. In accordance with the initial conditions, at the initial moment, the water level height is $+1$ meter. During the first hours of the solution, the liquid level gradually declines to the minimum of -1.68 m at $t = 17$ h. Thus, over 17 hours, the difference is 2.7 m. After that, an even sharper rise of the level is observed: at $t = 24$ h, the height of the water level reaches $+1.7$ m, which means that during 7 hours the water level rose by over 3 m. The rising level poses a serious risk for both the port and the city. We note that the second maximum is significantly higher than the first one, i.e., the seiche current completing its circle brings the enlarged water mass into Taganrog Bay. After the surge, the water
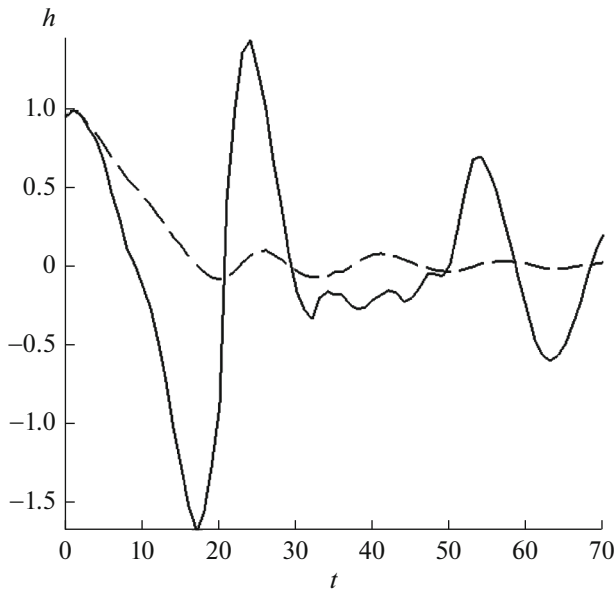
Fig. 6. Sea level evolution h in time in Taganrog. Time in hours is plotted along the abscissa axis. Dashed line corresponds to the solution in the presence of friction.
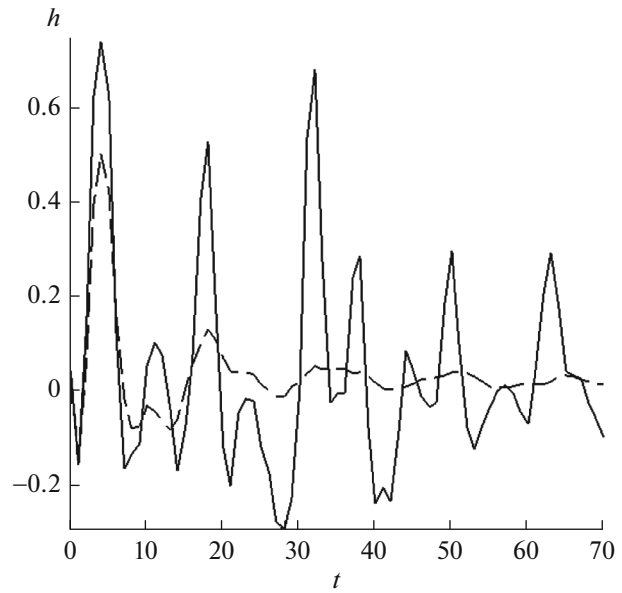

Fig. 7. Sea level evolution h in time in Berdyansk. Time in hours is plotted along the abscissa axis. Dashed line corresponds to the solution in the presence of friction.
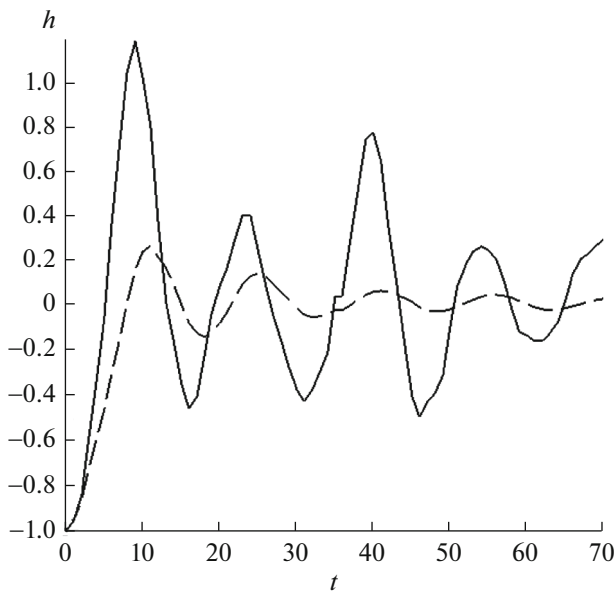

Fig. 8. Sea level evolution h in time in Genichesk. Time in hours is plotted along the abscissa axis. Dashed line corresponds to the solution in the presence of friction.
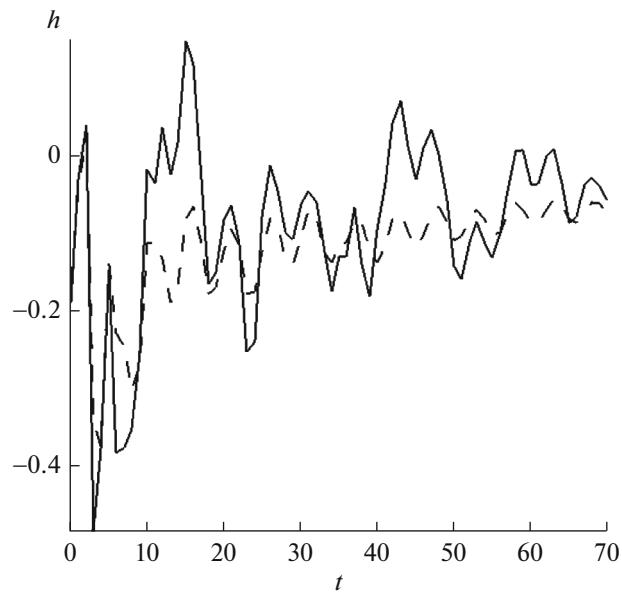

Fig. 9. Sea level evolution h in time in Kerch. Time in hours is plotted along the abscissa axis. Dashed line corresponds to the solution in the presence of friction.

leaves the bay much quicker and in 5 hours reaches the second minimum of −0.4 m. The next maximum +0.6 m is observed at $t = 53$ h, after which the water leaves the bay just as rapidly. Thus, the calculated seiche oscillations in Taganrog show sharp, large water level variations.

Moving from the east to the west, we study the situation in Berdyansk, Ukraine, with coordinates $x = 162286$ m and $y = 211211$ m. The graph presented in Fig. 7 shows the height of the sea level. At the initial moment, the sea level is close to equilibrium. Then in three hours, at $t = 4$ h, a sharp peak emerges
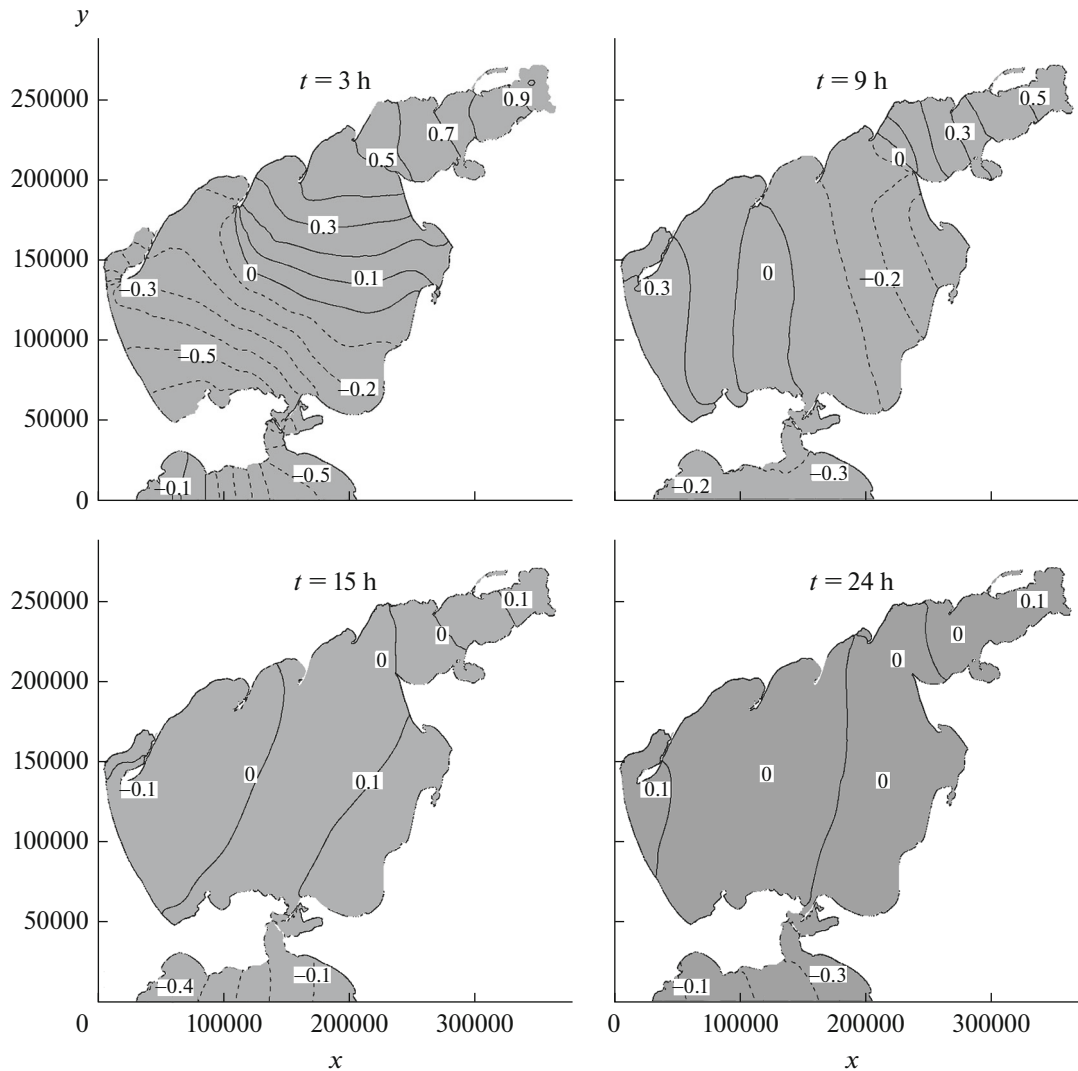
Fig. 10. Deviation η of the surface level from the equilibrium in the Azov Basin, friction force taken into consideration.

with the maximum of +0.75 m. After that an additional, gentler sloped maximum of +0.15 m is observed at $t = 12$ h. This situation repeats in time: the next major maximum appears at $t = 18$ h, and the collateral peaks come at $t = 24$ h, $t = 32$ h, and $t = 38$ h, after which the oscillation profile changes slightly: first gentler sloped peaks occur at $t = 44$ h and $t = 58$ h, followed by the sharper peaks at $t = 51$ h and $t = 65$ h. The presence of the secondary maximum is connected with the reflection of the current from the western coast of the Sea of Azov. The second principal maximum emerges when the water mass completes its full circle around the water area of the Sea of Azov; therefore, the period of oscillations for Berdyansk is about 13 hours. The third maximum is formed similarly, but it is higher than the second one due to the water entering from Taganrog Bay, where the fluctuation period is about 24−26 hours.

Moving to the west, let us study the situation in Genichesk with coordinates $x = 7491$ m and $y = 149229$ m. The city is positioned not directly on the Azov coast but on the bank of the Ulyutski estuary. The height profile of the sea level is shown in Fig. 8. It is similar to that of Berdyansk. However, this graph shows purer oscillations, without noise. This is stipulated by the geographical position of the city on the estuary bank, since the water masses reflected from the opposite coast do not reach here. The oscillation period is 15 hours. The third peak of the graph is significantly higher than the second one due to the inflow of the water mass from Taganrog Bay.

Let us study the sea level oscillations in the Kerch Strait with coordinates $x = 138847$ m and $y = 56282$ m, Fig. 9. The graph shows the increased noise and an insignificant rise of the sea level compared with the similar graphs plotted for other cities, which means that the seiches are quite rare in the Kerch Strait.

Thus, the intrinsic seiche oscillations with the initial amplitude of 1 meter in the Sea of Azov have been studied. The periods of oscillations determined at the characteristic points are 12 to 16 hours in the major ports of the Sea of Azov and 24−28 hours in Taganrog Bay. The small velocities and currents related to the seiche waves are found near the cities. The numerical calculations show that the seiche current does not penetrate into the Kerch Strait. Note that rise in the sea level in Taganrog, Genichesk, and Primoro-Akhtarsk can be considerable.

Let us study the same problem taking friction forces into consideration, for example, see [2]. We assume coefficient μ to be 2.6×10^{-3} according to [8].

The distributions of the water level at four characteristic time moments $t = 3, 9, 15,$ and 24 hours from the moment of the start of the oscillations are displayed in Fig. 10. The general behavior of the seiche waves does not change. The friction force introduces additional attenuation into the system causing the oscillation amplitude to decrease by a factor of 8 over the period compared to the amplitudes without friction; the seiche fades completely over three periods. As for the sea level in the Azov ports, the oscillation period is constant, while the amplitudes of the oscillations and current velocities decrease significantly.

A graph of the sea level variations with time in Taganrog is presented in Fig. 6. The impact of the friction force reduces the outflow of the water mass from the bay and, according to Fig. 6, induces an overtone with a 17-hour period, whose presence is stipulated by the diversity of the coastline of the gulf and the bay. Note the visual differences between the graphs with and without a friction force. The maxima are more gently sloping than the version without friction. The greatest swing of the oscillations reaches 0.1 m and quickly fades with time.

Similar features of the current (without variations in the oscillation period) are also observed in other cities; see Figs. 7−9. Let us consider the situation in Genichesk, where pure seiche waves have been observed. The sea level profile is shown in Fig. 8. Strong attenuation is observed with the greatest oscillation swing of 0.21 m. The major maxima are slightly displaced rightwards in time, but the oscillation period is the same 16 hours.

Thus, the influence of the friction force on the solution of the problem of intrinsic seiche waves has been studied. The friction coefficient $\mu \sim 10^{-3}$ results in a noticeable attenuation of the solution: in periods 2−3, the Azov sea level reaches equilibrium.

The obtained results are generally consistent with the data of long-term observations [1] and the outcomes of the numerical simulation based on alternative approaches. Besides, the obtained calculation results show that the intrinsic attenuation of the finite-difference algorithm based on regularized shallow water equations is considerably lower than the natural dissipation caused by the friction of the seabed.

6. CONCLUSIONS

The proposed new method of the numerical simulations of flows is applicable to the sea area. The shallow water equations in flux form are taken as the basis describing the impact of the wind, the Earth's rotation (Coriolis force), the seabed topology, and the friction forces on the seabed. The system of regularized shallow water equations is used as the basis of the numerical algorithm. Due to regularization, additional dissipation emerges in the system of equations, which smoothens the numerical oscillations, which, in turn, enables us to apply the explicit finite-difference approximation of the equations by central differences.

The studied examples of currents in the waters of the Sea of Azov and the Kerch Strait show that the developed algorithm complies with a well-balanced condition; i.e., it does not induce noticeable artificial oscillations of the solution caused by seabed peculiarities.

This approach has been applied in the numerical simulation of seiche waves with the initial amplitude of one meter typical for the Sea of Azov. The time dependences of the emerging oscillations near the main Azov ports have been determined and the corresponding rate fields calculated. It is found that the seiches do not penetrate into the Kerch Strait; however, for some cities, for example, Taganrog and Genichesk, the level differentials can reach two meters.

It is shown that consideration of the friction forces with the friction coefficients known from the published literature shows a sharp attenuation of the solution, so that after 2—3 periods the sea level in the Sea of Azov reaches equilibrium. This comparison indicates that the intrinsic dissipation of the numerical algorithm is significantly lower than the natural dissipation related, in particular, to the friction on the seabed.

It is known that the dependence of the main features of the seiche wave (period, height) on the initial distribution of the height level is rather weak, since they are mainly determined by the initial height difference. Here an example of the problem with the typical uniform initial height difference is presented. Besides, variants have been calculated with a nonlinear distribution of the initial height level determined by the impact of the real wind taken from the observational data. The results obtained are generally consistent with the data presented in the work, but have not been included in the paper due to their huge volume.

The simplicity and precision of the numerical algorithm proposed by the authors, together with the low computational costs and opportunities of implementation in parallel, as well as the untapped reserves of this method dealing with the unstructured grids and problems covering drying and flooding zones, make the algorithm competitive compared to the existing expensive methods of higher orders.

ACKNOWLEDGMENTS

REFERENCES

1. S. F. Dotsenko and V. A. Ivanov, *Natural Catastrophes in Azov-Black Sea Region* (Morsk. Gidrofiz. Inst., NAN Ukrainy, Sevastopol, 2010) [in Russian].

2. V. B. Zalesny, A. V. Gusev, and S. N. Moshonkin, "Numerical model of the hydrodynamics of the Black Sea and the Sea of Azov with variational initialization of temperature and salinity," Izv. Atmos. Ocean. Phys. **49**, 642—658 (2013).

3. V. B. Zalesny, N. A. Diansky, V. V. Fomin, et al., "Numerical model of the circulation of the Black Sea and the Sea of Azov," Russ. J. Numer. Anal. Math. Model. **27**, 95—111 (2012).

4. V. V. Fomin, A. A. Polozok, and R. V. Kamyshnikov, "Wave and storm surge modelling for Sea of Azov with use of swan+adcirc," in *Geoinformation Sciences and Environmental Development: New Approaches, Methods, Technologies, Proceedings of the 2nd International Conference, Limassol, Cyprus* (Rostov-on-Don, 2014), pp. 111—116.

5. G. G. Matishov and Yu. I. Inzhebeikin, "Numerical study of the Azov Sea level seiche oscillations," Oceanology **49**, 45-452 (2009).

6. Yu. G. Filippov, "Natural fluctuations of the Sea of Azov level," Russ. Meteorol. Hydrol., No. 37, 126—129 (2012).

7. A. I. Sukhinov and A. E. Chistyakov, "Parallel implementation of a three-dimantional hydrodynamic model of shallow water basins on supercomputing systems," Vychisl. Metody Programm. **13**, 290—297 (2012).

8. L. A. Krukier, "Mathematical modelling of Azov sea gydrodynamics for projects of damb building," Mat. Model. **3** (9), 3—20 (1991).

9. http://oceanography.ru/index.php/ru/component/jdownloads/viewdownload/6-/69.

10. O. V. Bulatov and T. G. Elizarova, "Regularized shallow water equations and an efficient method for numerical simulation of shallow water flows," Comput. Math. Math. Phys. **51**, 160—173 (2011).

11. O. V. Bulatov and T. G. Elizarova, "Regularized shallow water equations for numerical simulation of flows with a moving shoreline," Comput. Math. Math. Phys. **56**, 661—679 (2016).

12. T. G. Elizarova and D. S. Saburin, "Numerical simulation of fluid oscillations in fuel tanks," Math. Models Comput. Simul. **5**, 470—478 (2013).

13. T. Elizarova and D. Saburin, "Mathematical modeling and visualization of the sloshing in the ice-breaker's tank after impact interaction with ice barrier," Sci. Visualiz. **5** (4), 118—135 (2014).

14. T. G. Elizarova, M. A. Istomina, and N. K. Shelkovnikov, "Numerical simulation of solitary wave generation in a wind-water annular tunnel," Math. Models Comput. Simul. **4**, 552—559 (2012).

15. G. I. Marchuk, V. P. Dymnikov, and V. B. Zalesny, *Mathematical Models in Geophysical Fluid Dynamics and Numerical Methods of their Realization* (Gigrometeoizdat, Leningrad, 1967) [in Russian].

16. N. A. Dianskii, *Simulations of Ocean Circulation and Study of its Reaction on Short- and Long-Period Atmospheric Actions* (Fizmatlit, Moscow, 2013) [in Russian].

17. N. E. Voltsinger and R. V. Pyaskovskii, *Shallow Water Theory. Oceanology Problems and Numerical Methods* (Gidrometeoizdat, Leningrad, 1977) [in Russian].

18. T. G. Elizarova, *Quasi-Gas Dynamic Equations* (Springer, Berlin, Heidelberg, 2009; Nauchn. Mir, Moscow, 2007).

19. Yu. V. Sheretov, *Continuous Media Dynamics with Spatial-Temporal Averaging* (Regular. Khaotich. Dinamika, Moscow, Ishevsk, 2009) [in Russian].

20. B. N. Chetverushkin, *Kinetic Schemes and Quasi-Gasdynamic System of Equations* (CIMNE, Barcelona, 2008).

21. A. A. Zlotnik, "Energy equalities and estimates for barotropic quasi-gasdynamic and quasi-hydrodynamic systems of equations," Comput. Math. Math. Phys. **50**, 310−321 (2010).

22. Yu. V. Sheretov, *Regularized Hydrodynamics Equations* (Tversk. Gos. Univ., Tver, 2016) [in Russian].

Translated by N. Semenova